An alternative explanation of the semiarid urban area "oasis effect"

M. Georgescu,[1] M. Moustaoui,[1] A. Mahalov,[1] and J. Dudhia[2]

Received 12 August 2011; revised 10 October 2011; accepted 12 October 2011; published 22 December 2011.

[1] This research evaluates the climatic summertime representation of the diurnal cycle of near-surface temperature using the Weather Research and Forecasting System (WRF) over the rapidly urbanizing and water-vulnerable Phoenix metropolitan area. A suite of monthly, high-resolution (2 km grid spacing) simulations are conducted during the month of July with both a contemporary landscape and a hypothetical presettlement scenario. WRF demonstrates excellent agreement in the representation of the daily to monthly diurnal cycle of near-surface temperatures, including the accurate simulation of maximum daytime temperature timing. Thermal sensitivity to anthropogenic land use and land cover change (LULCC), assessed via replacement of the modern-day landscape with natural shrubland, is small on the regional scale. The WRF-simulated characterization of the diurnal cycle, supported by previous observational analyses, illustrates two distinct and opposing impacts on the urbanized diurnal cycle of the Phoenix metro area, with evening and nighttime warming partially offset by daytime cooling. The simulated nighttime urban heat island (UHI) over this semiarid urban complex is explained by well-known mechanisms (slow release of heat from within the urban fabric stored during daytime and increased emission of longwave radiation from the urban canopy toward the surface). During daylight hours, the limited vegetation and dry semidesert region surrounding metro Phoenix warms at greater rates than the urban complex. Although prior work has suggested that daytime temperatures are lower within the urban complex owing to the addition of residential and agricultural irrigation (i.e., "oasis effect") we show that modification of Phoenix's surrounding environment to a biome more representative of temperate regions eliminates the daytime urban cooling. Our results indicate that surrounding environmental conditions, including land cover and availability of soil moisture, play a principal role in establishing the nature and evolution of the diurnal cycle of near-surface temperature for the greater Phoenix, Arizona, metropolitan area relative to its rural and undeveloped counterpart.

Citation: Georgescu, M., M. Moustaoui, A. Mahalov, and J. Dudhia (2011), An alternative explanation of the semiarid urban area "oasis effect", *J. Geophys. Res.*, *116*, D24113, doi:10.1029/2011JD016720.

1. Introduction

[2] Anthropogenic land use and land cover change (LULCC) can have an impact on the overlying climate via alteration of the radiation budget and modification of the surface energy balance. A change in surface albedo can alter the amount of radiative energy absorption while vegetation abundance and water availability (e.g., regions of relatively high soil moisture) assist in the redistribution of incoming energy into latent and sensible heating back into the atmosphere [*Pielke*, 2001]. Urbanization is an extreme manifestation of anthropogenic LULCC that can further modulate the near-surface climate [*Oke*, 1987], and by means of a phenomenon known as the urban heat island (UHI) effect has been shown to increase urban relative to rural near-surface temperatures [*Bornstein*, 1968; *Oke*, 1973; *Landsberg*, 1981]. Large-scale urbanization, resulting from changes in associated surface properties, can therefore influence local-to-regional-scale climates by modifying the dynamic and thermodynamic properties of a region.

[3] The UHI effect has been the subject of research for many years [*Arnfield*, 2003; *Brazel et al.*, 2000; *Gedzelman et al.*, 2003; *Hawkins et al.*, 2004; *Oke and Maxwell*, 1975; *Sailor*, 1995; *Taha et al.*, 1991; *Taha*, 1997; *Tarleton and Katz*, 1995; *Tran et al.*, 2006; *Zhou et al.*, 2004]. Generally regarded as an evening and nighttime phenomenon [*Oke*, 1987], the UHI has also been shown to influence

[1]School of Mathematical and Statistical Sciences, Center for Environmental Fluid Dynamics, Global Institute of Sustainability, Arizona State University, Tempe, Arizona, USA.
[2]Mesoscale and Microscale Meteorology Division, National Center for Atmospheric Research, Boulder, Colorado, USA.

0148-0227/11/2011JD016720

daytime temperatures [e.g., *Tran et al.*, 2006] and, in some cases, to have a daytime signature that exceeds that of its nighttime counterpart [e.g., *Cheval and Dumitrescu*, 2009].

[4] Urban canyon geometry plays a key role in regulating both the daytime and nighttime UHIs [*Oke*, 1981]. Because of the reduction of unobstructed visible sky within an urban canopy, longwave radiation loss is reduced after sunset, leading to greater near-surface temperatures relative to rural environs during evening and nighttime hours. The geometric configuration of urban areas can have the opposite effect during daytime, as incoming radiation is reduced because of shading effects [*Oke*, 1987]. The greater heat capacity of the built environment can further intensify the nighttime UHI as stored energy is slowly released during the night [*Grimmond and Oke*, 1999].

[5] During daylight hours, the presence of urban parks can decrease local temperatures [*Spronken-Smith et al.*, 2000] by means of repartitioning toward greater latent as opposed to sensible heating, leading to an oasis effect [*Oke*, 1987]. The oasis effect (i.e., repartitioning toward greater latent heating because of the presence of irrigated lawns, parks, etc.) has been proposed as a likely mechanism for lower urban daytime temperatures over semiarid cities (e.g., Phoenix, Arizona) compared with the surrounding semidesert environment [*Brazel et al.*, 2000; *Golden et al.*, 2006; *Stabler et al.*, 2005], although debate as to the existence and extent of this mechanism continues [*Fast et al.*, 2005]. It is possible that the oasis effect depends on individual city characteristics, including urban morphology, building design, and structured materials used, as well as time of season and particular climatic regimes [*Potchter et al.*, 2006]. That the oasis effect has a local impact is not in question [*Spronken-Smith et al.*, 2000], but whether local cooling by means of this mechanism scales beyond the microscale is an important subject that warrants attention. Research addressing the existence and mechanism of the semiarid urban area daytime cool island phenomenon is essential for land use and city planners, energy producers, and inhabitants of semiarid cities, requiring improved understanding of the principal consequences of continued LULCC and associated urbanization.

[6] Urban complexes located in semiarid regions, such as the geater Phoenix, Arizona, metropolitan area, are particularly vulnerable as UHI-related impacts aggravate the already severe nature of semiarid environments. Water sustainability concerns resulting from rising demands that are due to population increase [*Gober and Kirkwood*, 2010] and projected impacts from large-scale anthropogenic climate change on large watersheds such as the Colorado River Basin [e.g., *Barnett and Pierce*, 2008; *Rajagopalan et al.*, 2009] requires a fundamental understanding of impacts (e.g., effects on the diurnal cycle of near-surface temperature) resulting from continued urbanization in these already-stressed environments.

[7] The Phoenix metropolitan area, located in the semiarid Sonoran desert of the southwestern United States, has witnessed extensive land surface modification since the middle of the previous century [*Knowles-Yanez et al.*, 1999; *Georgescu et al.*, 2009], with considerable impacts on near-surface temperatures [*Brazel et al.*, 2000]. Analysis of historical temperature records indicates that Phoenix exemplifies among the most extreme instances of urban-induced warming [*Hansen et al.*, 1999]. Of particular concern is the region's ever-increasing urban heat island (UHI) intensity [*Hsu*, 1984; *Balling and Brazel*, 1987; *Brazel et al.*, 2000], resulting from unrelenting development and urbanization. Consequences for UHI enhancement extend beyond the climate realm, raising air quality [*Balling et al.*, 2001; *Jacobson*, 2010], ecological [*Grimm and Redman*, 2004], social [*Harlan et al.*, 2008], and sustainability [*Gober and Kirkwood*, 2010] concerns. Further growth into a megapolitan complex known as the Sun Corridor is projected to bring the region's population total to near 10 million by 2040 [*Gammage et al.*, 2008]. Monitored and sustainable expansion is therefore required [*Grimm et al.*, 2008], and impact assessment of historical urban development and growth is a key step toward ensuring minimum climate-ecosystem impacts of the region's relentlessly expanding urban footprint.

[8] The principal aim of the current study is to evaluate the ability of the Weather Research and Forecasting System (WRF), applied over the semiarid Phoenix metropolitan area, to accurately represent the evolution of the diurnal cycle of near-surface temperatures. A key question relates to the principal mechanism(s) responsible for the urban area's daytime cool island. By focusing on an individual urban hub, this work is likely to shed further light on precise local-to-regional-scale consequences associated with urban expansion. Our objective is to build upon previous work, focusing on improving our understanding of the development of the diurnal cycle of near-surface temperatures [e.g., *Zehnder*, 2002; *Grossman-Clarke et al.*, 2005; *Georgescu et al.*, 2008, 2009] to better characterize impacts of urbanization and better illustrate the sensitivity of local-to-regional-scale climate to LULCC over this semiarid metropolitan complex. We focus on the summertime climatic evolution of the Phoenix diurnal cycle of near-surface temperatures, which is of significant importance to millions of the region's inhabitants, as stress levels (indicated by combined effects of extreme temperatures and moisture levels) are at their maximum during this time of year [*Golden et al.*, 2008].

2. Methods

2.1. RCM Model Used: WRF-ARW

[9] We have used version 3.2.1 of the WRF [*Skamarock et al.*, 2008; *Skamarock and Klemp*, 2008] modeling system to conduct high-resolution (2 km grid spacing within the innermost domain) sensitivity experiments to anthropogenic LULCC over the semiarid Phoenix metropolitan area. The ability of WRF to reproduce the region's midsummer climate was evaluated against appropriate observations (see section 2.2). A detailed description and inventory of options utilized, including domain extent, forcing data, parameterization options, and irrigation application are presented below.

[10] WRF is a fully compressible, nonhydrostatic model that has been used for a variety of applications, ranging from local to global scales. We initialized and forced WRF, at the lateral boundaries, with data obtained from the North American Regional Reanalysis (NARR) data set [*Mesinger et al.*, 2006]. Simulations for all experiments were initialized on 30 June, 00:00 UT, of the respective year and concluded on 31 July, 12:00 UT, of the respective year. We used three nested grids, centered over the Phoenix Sky Harbor International Airport (Figure 1a).

[11] The four-layer Noah land surface model (LSM) [*Chen and Dudhia*, 2001] was used as the land surface

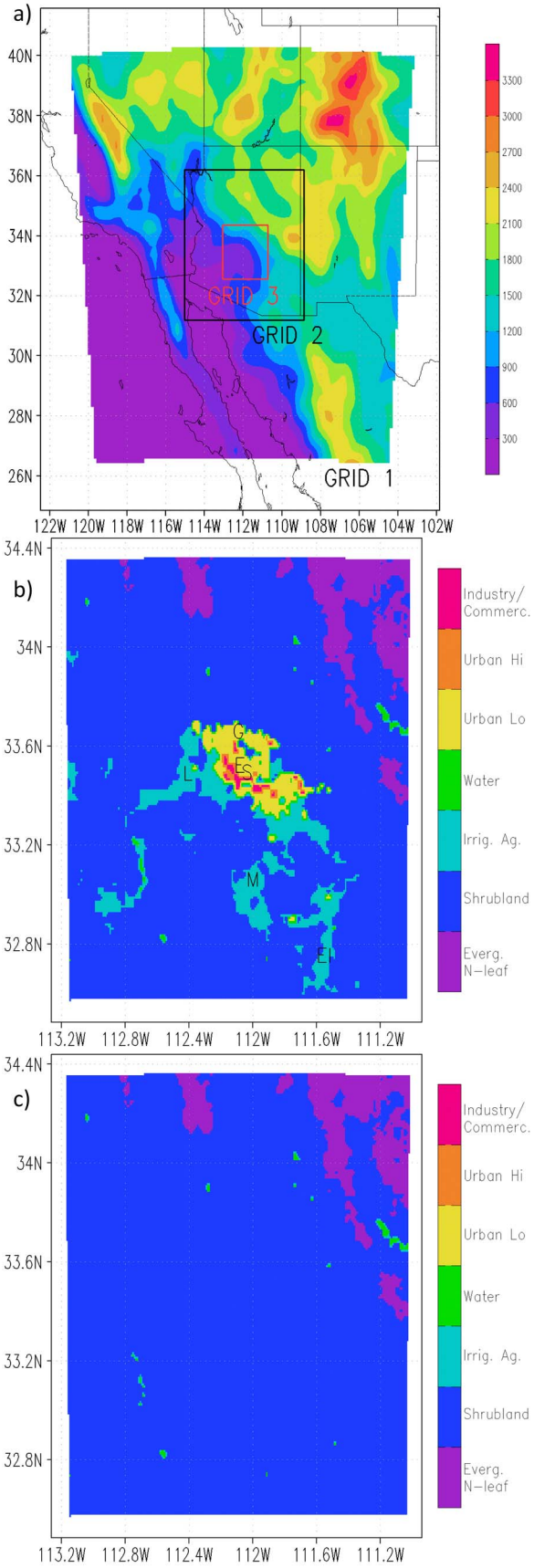

component of WRF to update soil temperature and moisture following model initialization. The Noah LSM scheme has been widely used in the regional climate modeling community as an operational scheme at the National Centers for Environmental Prediction (NCEP), in the development of the 25 year NARR data set [*Mesinger et al.*, 2006], and as part of an international program focused on producing future regional climate change assessments (North American Regional Climate Change Assessment Program: http://narccap.ucar.edu/data/rcm-characteristics.html). To better account for urban-related processes, we made use of the single-layer Noah Urban Canopy Model (UCM) [*Kusaka and Kimura*, 2004], which has been evaluated in both coupled [*Lo et al.*, 2007] and uncoupled modes [*Loridan et al.*, 2010].

[12] The U.S. Geological Survey's (USGS) 21 class, 30 m 1992 National Land Cover Data set (NLCD92) [*Vogelmann et al.*, 2001] was used to represent modern-day LULC within the Noah LSM. The landscape classification scheme used is presented in Table 1.

[13] Irrigated agriculture was accounted for by setting the volumetric water content of cropland category pixels (class 12 in Table 1; see also Figure 1b), for all soil layers, to soil saturation as a function of the green vegetation fraction (i.e., water is not added to bare soil for which vegetation is lacking). Notwithstanding the semiarid nature of the region, the major crops of Maricopa County (home to the Phoenix metro area) include cotton (growing season ranges from April to October), vegetables (e.g., soybean; growing season ranges from June through late fall), and orchards used for oranges and grapefruits (annual growing season). In each case, significant irrigation is required for crop growth. For example, at full blossom peak (i.e., during midsummer), cotton requires up to 25 mm day^{-1} of irrigation water [*Erie et al.*, 1982]. Irrigation was set at a frequency of once daily for cropland category pixels. A simple drip-style irrigation scheme was implemented for the low-intensity residential class within WRF to account for the region's common method of mesic landscaping. Every third day, the second (10–40 cm depth) and third (40–100 cm depth) soil layers of the Noah LSM corresponding to this urban class were set to a reference volumetric soil moisture (i.e., threshold below which transpiration begins to stress but above wilting point) level, also as a function of the green vegetation fraction. The green vegetation fraction for each grid cell was based on a monthly, 5 year, 0.144°, climatological data set assumed valid on the 15th of the month [*Gutman and Ignatov*, 1998] and interpolated to daily values. Albedo was accounted for by means of inclusion of a monthly, 5 year, 0.144°, climatological data set assumed valid on the 15th of the month, also interpolated to daily values [*Csiszar and Gutman*, 1999].

Figure 1. (a) Domain extent and geographical representation of the WRF nested grid configuration with topography (in meters) overlaid. (b) NLCD92 landscape representation of grid 3 used in WRF simulations. Individual station locations used to evaluate WRF are marked: E, Encanto; G, Greenway; S, Sky Harbor International Airport; L, Litchfield; El, Eloy; M, Maricopa. (c) Pre-Settlement landscape representation of grid 3 used in WRF simulations.

Table 1. LULC Categories Used for Noah LSM

LULC	Noah
1	Evergreen Needleleaf
2	Evergreen Broadleaf
3	Deciduous Needleleaf
4	Deciduous Broadleaf
5	Mixed Forests
6	Closed Shrublands
7	Open Shrublands
8	Woody Savannas
9	Savannas
10	Grasslands
11	Permanent Wetland
12	Croplands
13	Cropland or Natural Vegetation Mosaic
14	Snow and Ice
15	Barren or Sparsely Vegetated
16	Ocean
17	Wooded Tundra
18	Mixed Tundra
19	Bare Ground Tundra
31	Urban Low-Intensity Residential
32	Urban High-Intensity Residential
33	Urban Commercial or Industrial

2.2. Experiments Performed

[14] We used a nested grid configuration with all three grids centered over the Phoenix Sky Harbor International Airport (Figure 1a). The finest grid (grid 3) utilized a spacing of 2 km in the horizontal direction, with increasing mesh size for the intermediate (grid 2; 8 km) and coarsest grid (grid 1; 32 km) (Figure 1b). It is important to note that our intent is not to capture effects of individual urban elements within the built environment, but to resolve the land-atmosphere interactions and associated dynamics relevant to the local-to-regional scale LULCC for the metropolitan region. We made use of a modified version of the Kain-Fritsch convective parameterization scheme to represent convective processes on the coarsest grid only [*Kain*, 2004] and represented convective motions explicitly on grids 2 and 3.

[15] Guided by previous research, we restricted our WRF *sensitivity* (to LULCC) experiments to separate dry monsoon seasons, as the impact of the land surface may more readily be distinguished during such regimes [e.g., *Anyah et al.*, 2008; *Georgescu et al.*, 2008, 2009]. In fashioning our experimental design this way, we simulated three different Julys, corresponding to three different years (thus accounting for interannual variability) using two different land cover representations (Table 2). Monsoon season selection was based on NARR data availability (1979 to present day) and analysis of the Daily Unified Precipitation data set [*Higgins et al.*, 2000]. July months corresponding to 1979, 1989, and 1994 were chosen (Table 2). The precise methods and selection criteria used are discussed in detail by *Georgescu* [2008].

[16] Modern-day urban areas were represented via use of the 1992 USGS-derived 30 m NLCD92 data set [*Vogelmann et al.*, 2001] (see section 2.1 for details). Produced as part of Federal Region 9 (which includes the states of Arizona, California, and Nevada), the Arizona portion of the NLCD92 data set was based on satellite imagery obtained between the late 1980s and early 1990s. The region's LULC representation was therefore based on this same time, and we selected the month-year of model evaluation (July 1990) to be consistent with the timing of underlying land surface representation.

[17] A hypothetical land surface was developed by replacing all anthropogenic pixels (this consisted of three different categories of urban land use and irrigated agriculture; see also Table 1) with native vegetation (i.e., shrubland; hereafter presettlement) (Figure 1c). Monthly mean differences between the three (July) simulations with the NLCD92 and presettlement landscape scenarios (referred to as *ensemble* differences for the purpose of this study) enabled direct comparison of midsummer climate sensitivity to anthropogenic landscape change.

2.3. Observational Data

[18] The source of near-surface temperature data against which WRF was evaluated is described below.

[19] We make use of five regional stations available from the Arizona Meteorological Network (AZMET: http://ag.arizona.edu/azmet) and a sixth station, Phoenix Sky Harbor International Airport (the only first-order National Weather Service station in the region), courtesy of the National Climatic Data Center. Of the six stations, three are urban stations (Phoenix Encanto, Phoenix Greenway, and Sky Harbor International Airport) while the remaining three are located outside the metropolitan area (Eloy, Litchfield, and Maricopa). The locations of each station relative to one another and the boundary walls of the innermost grid are shown in Figure 1b. It is important to note that although our experiments are high resolution in nature (2 km on the innermost grid), one cannot expect exceptional agreement between a model-resolved 4 km^2 grid cell and a station location covering an area of 1 m^2. For this reason, observations are averaged over all (six) stations and compared with the corresponding average of model-simulated, nearest grid point station locations, from 1 July 1990 (12:00 UT) through 31 July 1990 (12:00 UT). We discard the initial 36 simulation hours and utilize this time period as model spin-up. Observational data availability with a temporal frequency of 3 h and equivalent model output generation allows for assessment of the diurnal cycle.

3. Results

3.1. Evaluation of WRF

[20] We begin evaluation of WRF's performance via comparison against near-surface temperature observations (see section 2.3 above). WRF performs reasonably during the course of the month, tracking the day-to-day variability of near-surface temperatures with notable fidelity (Figure 2). The generally well-simulated daytime warming is balanced

Table 2. Summary of Experiments Performed[a]

Landscape Representation	WRF[b]
NLCD92	1990[c]
NLCD92	1979, 1989, 1994
Presettlement	1979, 1989, 1994

[a]For each experiment, the analysis time consists of the period lasting from 1 July, 12:00 UT, through 31 July, 12:00 UT.

[b]Years from which initial and lateral boundary conditions were used to force WRF in June/July.

[c]Denotes experiment used as control simulation and evaluated against observations.

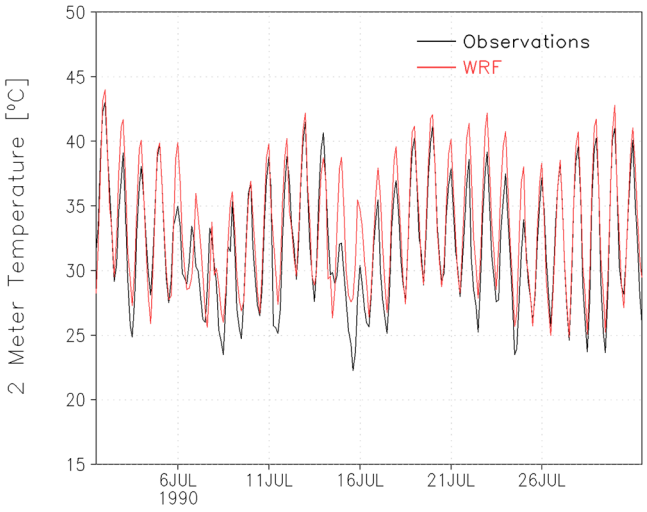

Figure 2. Observed (black contour) and WRF-simulated (red contour) 2 m air temperature for 1 July 1990 (12:00 UT)–31 July 1990 (12:00 UT).

by equally well-simulated nighttime cooling, resulting in a diurnal range that is of similar magnitude to observations. This difference is apparent when quantifying impacts on urban stations only (Table 3) (we assess impacts on urban stations only as it is these stations that are most influenced by utility of the UCM scheme). Although WRF does display a small warm bias over urban locales, the representation of the monthly averaged diurnal range of near- surface temperatures is well captured.

[21] The simulation of amplitudes and phases of the diurnal and monthly cycles of near-surface temperatures provides an ideal test bed for model parameterizations and representation of the interacting surface, boundary layer, and free atmosphere. To more fully examine WRF performance, the near-surface temperature profiles presented in Figure 2 are filtered to separate diurnal variations and longer period fluctuations. We apply a band-pass nonrecursive filter using a Kaizer window to avoid the Gibbs phenomenon [*Hamming*, 1983], spanning periods ranging between 18 and 30 h. The diurnal variability simulated by WRF closely follows the observed variability (Figure 3a). WRF is able to properly resolve both the timing of the diurnal cycle (Figure 3b) and the temperature fluctuations after applying a low-pass filter that removes all periods less than 30 h (Figure 3c).

[22] Figure 3b presents the composite, monthly averaged diurnal cycle for diurnal variations of temperature derived for both WRF and observations. These average cycles are calculated by selecting an hour during a day and averaging the temperature perturbation values found at that hour between different days of the month. The composite cycle illustrates the correct WRF-simulated evolution of the diurnal cycle, in a mean sense, including the timing of peak daytime temperatures. The standard deviation (Figure 3d) associated with the WRF-simulated cycle, with respect to observations, highlights the relative range of near-surface temperature uncertainty, depicting an envelope of model variability, relative to observations, within 1°C (Figure 3d).

[23] The relative performance of WRF on both diurnal and monthly time scales reflects the proper representation among interacting elements of the land-atmosphere system essential for achieving the correct amplitude and phase of these forced modes. In particular, an accurate representation of the evolving nature of the diurnal cycle serves as a key examination of many aspects of the model's physical parameterizations. Although it is beyond the scope of this paper, sensitivity of the simulated diurnal cycle over this semiarid region to the choice of physical parameterizations is an essential question that is the scope of future research.

3.2. Sensitivity to LULCC

[24] Guided by the well-represented diurnal cycle presented in the previous section, we next assess the impact of near-surface temperature sensitivity to LULCC. Near-surface temperature sensitivity to anthropogenic LULCC closely follows the pattern of landscape modification, with areas undergoing urbanization experiencing diurnally averaged warming that is partly offset by conversion to irrigated agriculture (Figure 4a). Warming and cooling impacts of LULCC largely offset each other in a regional sense. To account for the influence of LULCC on the monthly averaged diurnal cycle, we next present distinct land use conversion themes (e.g., examination of grid cells undergoing conversion from shrub (presettlement scenario) to urban (NLCD92) land) to evaluate how each cover's alteration has contributed to changes in the evolution of the diurnal cycle (Figure 4b). The simulated conversion of native shrubland to irrigated agriculture imparts a peak (daytime) cooling of −0.15°C. This impact (on the near-surface temperature) appears to be of secondary importance to that of urban development. The conversion of native shrubland to urban land drives two distinct and opposing impacts during the course of the diurnal cycle: cooling during the daytime hours and warming during the evening and nighttime hours (i.e., the well-known UHI effect). Mean evening and nighttime warming (peaking at 2.6°C) is partially offset by mean daytime cooling (peaking at −1.3°C) and results in an overall warming approaching 1°C for grid cells undergoing conversion to urban land.

[25] The accurate representation of the diurnal cycle and its agreement with observations (Figures 2 and 3 and section 3.1) provides confidence that the simulated daytime cooling (which emerges on the climatic timescale (Figure 4b)) resulting from urbanization is a robust feature, rather than a model artifact.

[26] Averaged daily variations of near-surface temperature differences (NLCD92-presettlement) for grid cells undergoing landscape conversion from shrubland to urban land are presented for midafternoon and late-afternoon time

Table 3. Mean Observed and WRF-Simulated Maximum, Minimum, and Difference Between Maximum and Minimum 2 m Air Temperature Across the Trio of Urban Stations[a]

	Observations	WRF
T_{mean}	32.9	33.7 (+0.8)
T_{Hi}	38.3	39.6 (+1.3)
T_{Lo}	27.6	28.3 (+0.7)
$T_{Hi} - T_{Lo}$	10.7	11.3 (+0.6)

[a]The number in parentheses denotes departure relative to observations. Analysis is for the period 1 July 1990 (12:00 UT) through 31 July 1990 (12:00 UT).

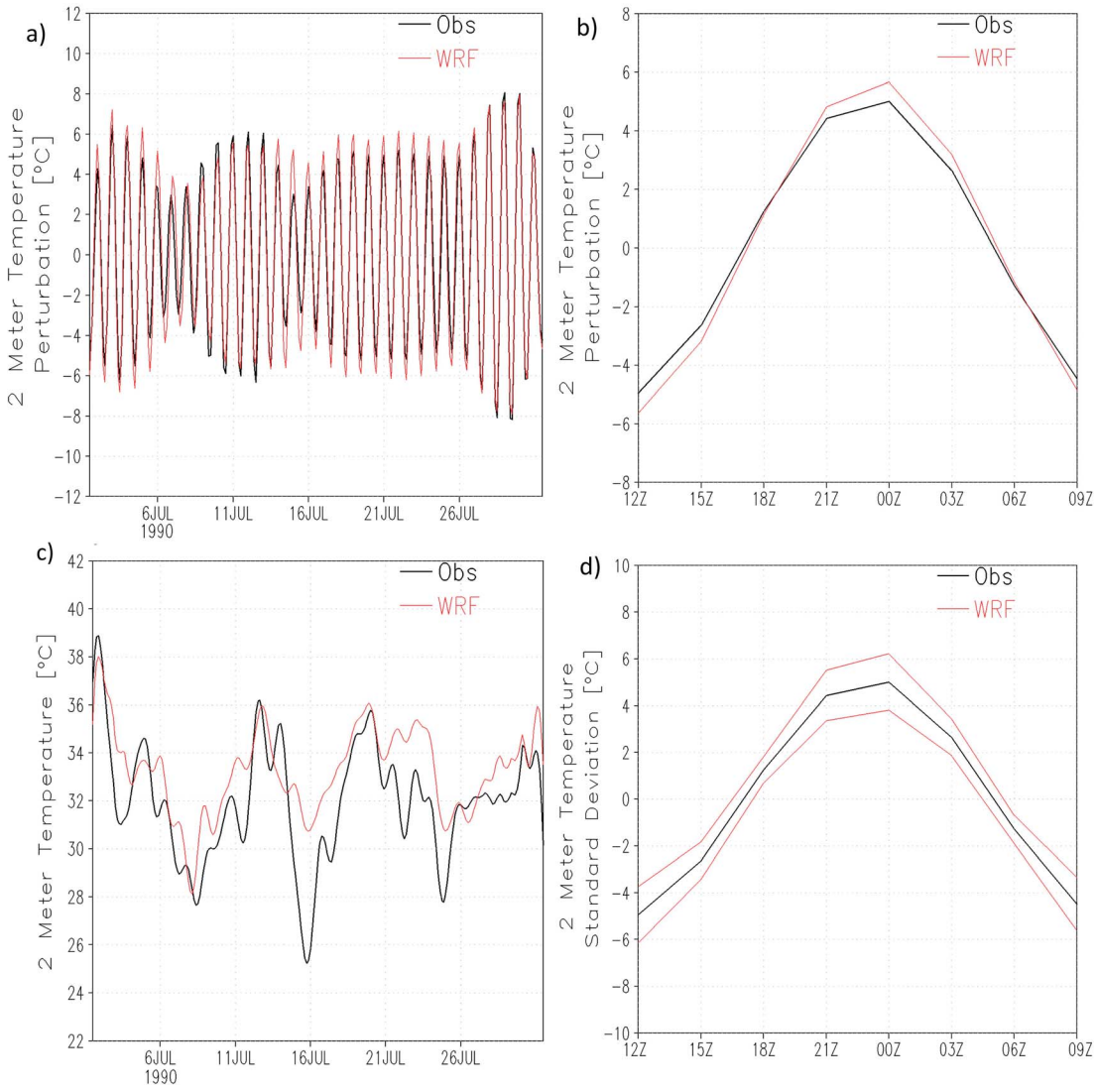

Figure 3. (a) Two meter air temperature perturbation, after applying a band-pass filter spanning the range between 18 and 30 h, for observations (black contour) and WRF (red contour). (b) Composite monthly averaged diurnal cycle of band-pass filtered 2 m air temperature for observations (black contour) and WRF (red contour). (c) As in Figure 3a, but after applying low-pass filter that removes all periods less than 30 h. (d) Simulated 2 m air temperature ±1 standard deviation of the composite monthly averaged diurnal cycle (red contours) relative to observations (black contour).

periods to illustrate the aforementioned daytime cooling and transition to urban warming that occurs during late afternoon and early evening (Figure 5a). Differences between NLCD92 and presettlement are greater for midafternoon hours (21:00 UT), with presettlement temperatures consistently warmer, by about 1°C, during the course of July. By late afternoon (00:00 UT), these differences are reduced by half, fluctuating between 0°C and 1°C during the course of the month (warmer for presettlement relative to NLCD92). Further support for this conclusion is available from previous observational analyses by *Brazel et al.* [2000], who document historical, negative, (May) urban minus rural near-surface maximum (i.e., daytime) temperature differences between a number of urban and residential stations and a small, rural town located ~25 km southeast of the metropolitan area that has remained mostly undeveloped [*Brazel et al.*, 2000, Figure 4c]. Although there are methodological differences in the (modeling) approach used in this paper and the approach used by *Brazel et al.* [2000] (entirely observational), their results explicitly illustrate the daytime urban area cooling relative to outlying desert locations (i.e., undeveloped land) that was simulated in our experiments. Figure 5b presents an analysis similar to that of Figure 5a, but for nighttime hours. Near-surface temperature differences between NLCD92 and presettlement are generally between 1.5°C and 3°C, highlighting the greater simulated warming impact of the nighttime UHI relative to daytime cooling . As before, additional observational support for this conclusion is available from prior analyses of observational data documenting positive nighttime temperature differences

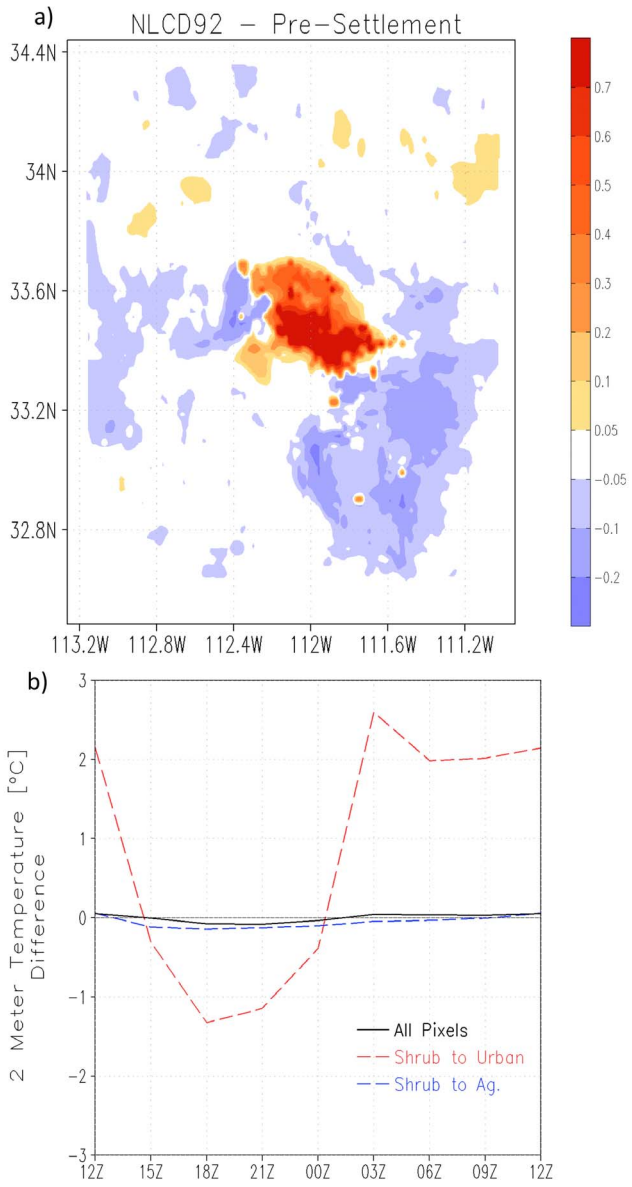

Figure 4. (a) WRF-simulated ensemble-averaged 2 m air temperature difference (°C) (monthly mean of NLCD92 members minus monthly mean of presettlement members). (b) WRF-simulated time series of diurnally averaged 2 m air temperature difference (°C) for grid cells undergoing conversion from shrub (presettlement scenarios) to urban (NLCD92 scenarios) (dashed red line), shrub (presettlement scenarios) to irrigated agriculture (NLCD92 scenarios) (dashed blue line), and all pixels (presettlement scenarios) to all pixels (NLCD92 scenarios) (solid black line).

between urban and surrounding desert landscapes [*Brazel et al.*, 2000, Figure 4d].

3.3. Impact of LULCC on Energy Balance

[27] We begin the discussion of the causes underlying impacts on the diurnal cycle of near-surface temperatures by examination of the energy balance components. Figure 6a presents monthly averaged sensible heat flux differences between the NLCD92 ensemble members and presettlement ensemble members. The pattern of landscape modification is evident, with the largest differences in sensible heating occurring over areas where land was modified from shrubland to irrigated agriculture and urban land (also compare with Figures 1b and 1c to note areas of anthropogenic LULCC). LULCC resulted in an overall decrease in sensible heating. For areas undergoing a conversion from semidesert to irrigated agriculture, the decrease in sensible heating was compensated by an increase in latent heating of similar magnitude (Figure 6b). The presence of soil water and irrigation, required to sustain agricultural productivity in this harsh environment, resulted in a repartitioning of energy toward enhanced latent heating. Differences in latent heat flux, however, were negligible over areas undergoing urbanization,

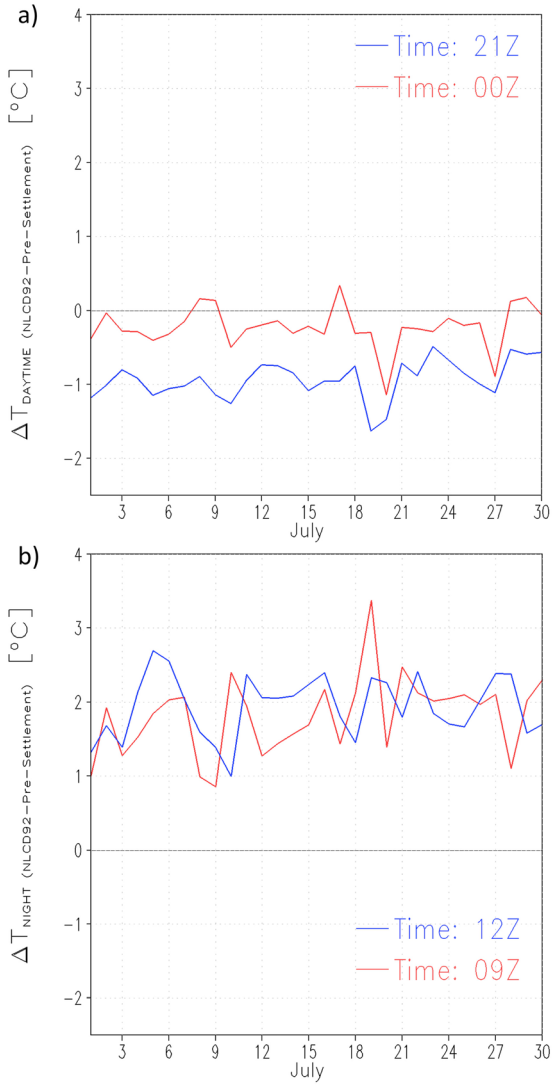

Figure 5. (a) WRF-simulated 2 m temperature difference for grid cells undergoing conversion from shrub (presettlement scenarios) to urban (NLCD92 scenarios) land during daytime, at 21:00 UT and 00:00 UT. (b) As in Figure 5a, but for nighttime at 09:00 UT (blue line) and 12:00 UT (red line).

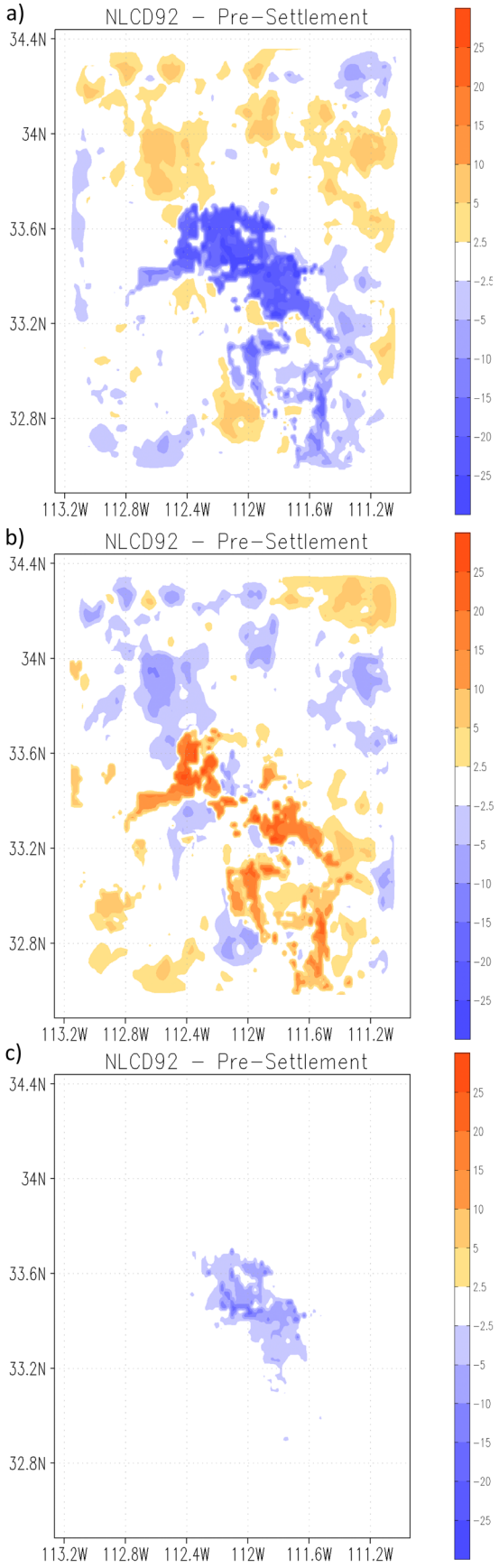

Figure 6. (a) Monthly averaged WRF-simulated sensible heat flux difference (mean of NLCD92 members minus mean of presettlement members). (b) As in Figure 6a, but for latent heat flux. (c) As in Figure 6a, but for ground heat flux. Units are W m^{-2}.

and normalizing against net all-wave radiation did not alter this conclusion (not shown). Turning off irrigation within the low-intensity residential area did not indicate any discernible influence on near-surface temperatures or on the components of the energy balance (not shown).

[28] In addition to repartitioning surface-absorbed energy between latent and sensible heating, the relatively high heat capacity of the urban fabric is responsible for storing a significant fraction of available energy [*Grimmond and Oke*, 1999]. Differences in monthly averaged ground heat flux between the NLCD92 and presettlement simulations are shown in Figure 6c. Negative differences indicate greater heat storage for NLCD92 relative to the presettlement simulations (ground heat flux is positive when directed away from the surface and negative when directed into the surface; greater negative values of ground heat flux are simulated for NLCD92 simulations relative to the presettlement experiments, resulting in the negative differences presented in Figure 6c). As the Sun rises each morning, rather than heating surface and near-surface air as would happen over the nondeveloped and sparsely vegetated surrounding semidesert, more of the incoming energy is lost through ground heat flux resulting from the physical mass of the built environment.

[29] The increase in urban heat storage (relative to the undeveloped semidesert), which occurs largely during daylight hours, results in increased sensible heat fluxes during the nighttime hours for NLCD92 relative to presettlement (Figure 7a). The slow release of stored energy is a principal factor for the urban-induced nighttime warming noted in the preceding section (see Figure 4b). The warmer nighttime urban canopy is also responsible for the increasing emission of longwave energy toward the surface (resulting from a reduction in the sky view factor, leading to a decrease in net longwave radiation loss to the atmosphere), although this effect appears to be largest over the industrial-commercial landscape and diminishes rapidly over lower-intensity residential areas (Figure 7b).

3.4. Daytime Cool Island

[30] The previous section discussed impacts of LULCC and associated urbanization on the surface energy balance but did not address possible reasons for the simulated daytime cooling effect besides heat storage within the urban infrastructure. That the built environment results in enhanced heat storage is not a distinguishing feature of semiarid cities relative to their temperate brethren [*Grimmond and Oke*, 1999]. Therefore, we next address the basis for the simulated daytime cooling resulting from urbanization.

[31] Figure 8 shows monthly averaged, WRF-simulated 2 m air temperatures across latitude band 33.5°N for the paired (i.e., NLCD92 and presettlement) simulations, for each of the trio of simulated Julys, at 11:00 local standard time (LST) (that time of day when the simulated cooling was greatest; see also Figure 4b). The particular latitude band

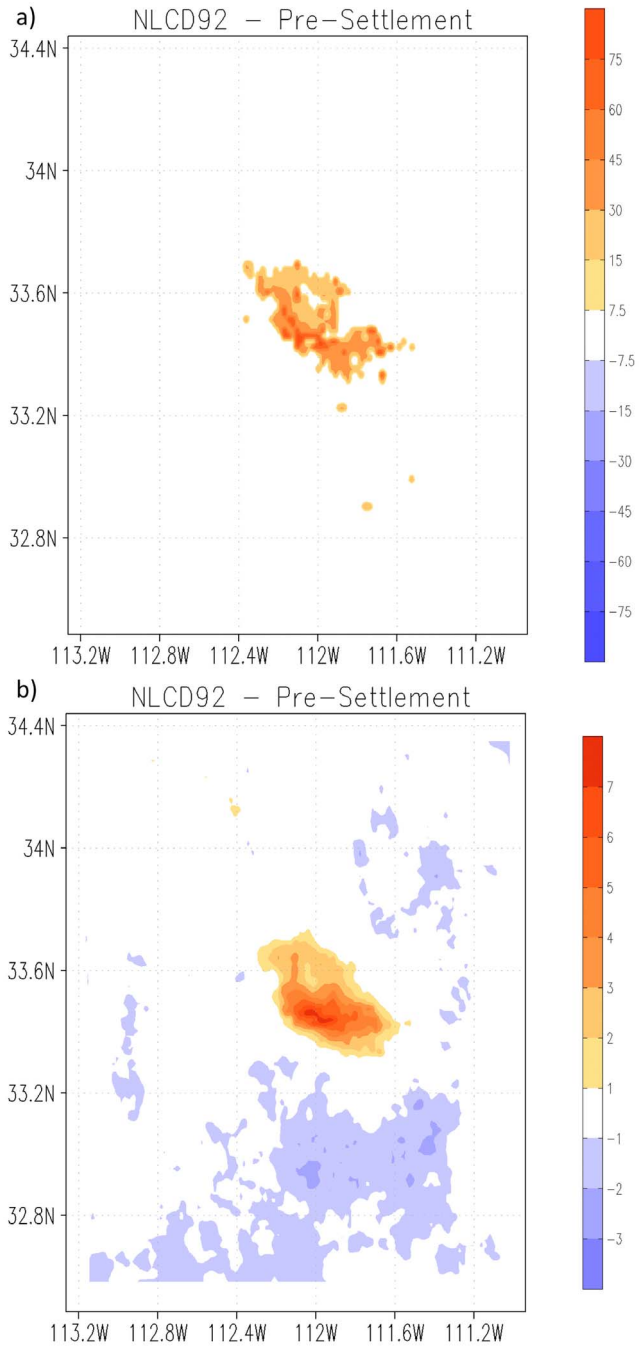

Figure 7. (a) As in Figure 6a, except for nighttime hours. (b) Nighttime simulated downward longwave flux difference at surface (mean of NLCD92 members minus mean of presettlement members). Nighttime hours: 20:00 LST–05:00 LST.

chosen crossed through the surrounding semidesert and traversed through the urban core. Diagnosing contrasting semidesert and urban impacts was deemed necessary, and deciding on latitude bands slightly north or south of 33.5°N did not modify the interpretation of our results.

[32] It is evident, from an assessment of Figure 8, that near-surface temperatures between the paired simulations are similar west of the anthropogenically modified landscape (along the selected transect, irrigated agriculture begins just east of about 112.5°W while the developed urban area starts at about 112.3°W; see also Figure 1b). The sharp decrease in near-surface temperatures for the paired simulations just east

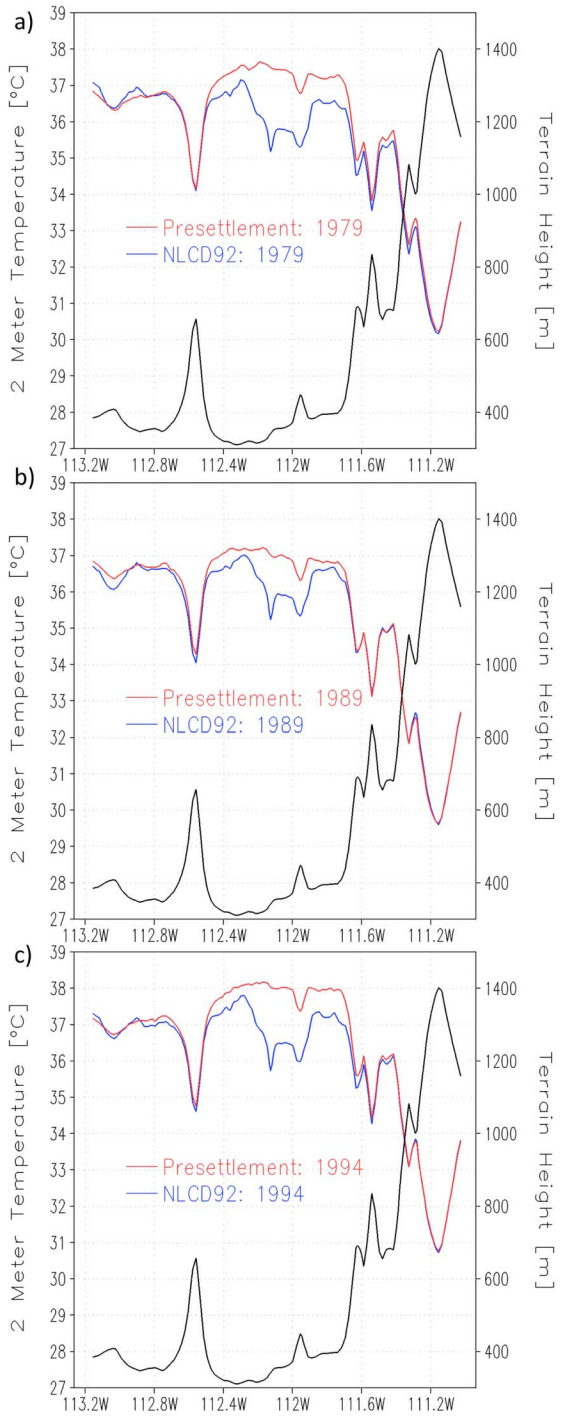

Figure 8. Monthly averaged WRF-simulated cross section of 2 m air temperature at 33.5°N at 11:00 LST for NLCD92 scenarios (solid blue line) and presettlement scenarios (solid red line) for (a) 1979, (b) 1989, and (c) 1994. The *y* axis on right-hand side represents varying terrain heights (solid black line) across a given latitude band.

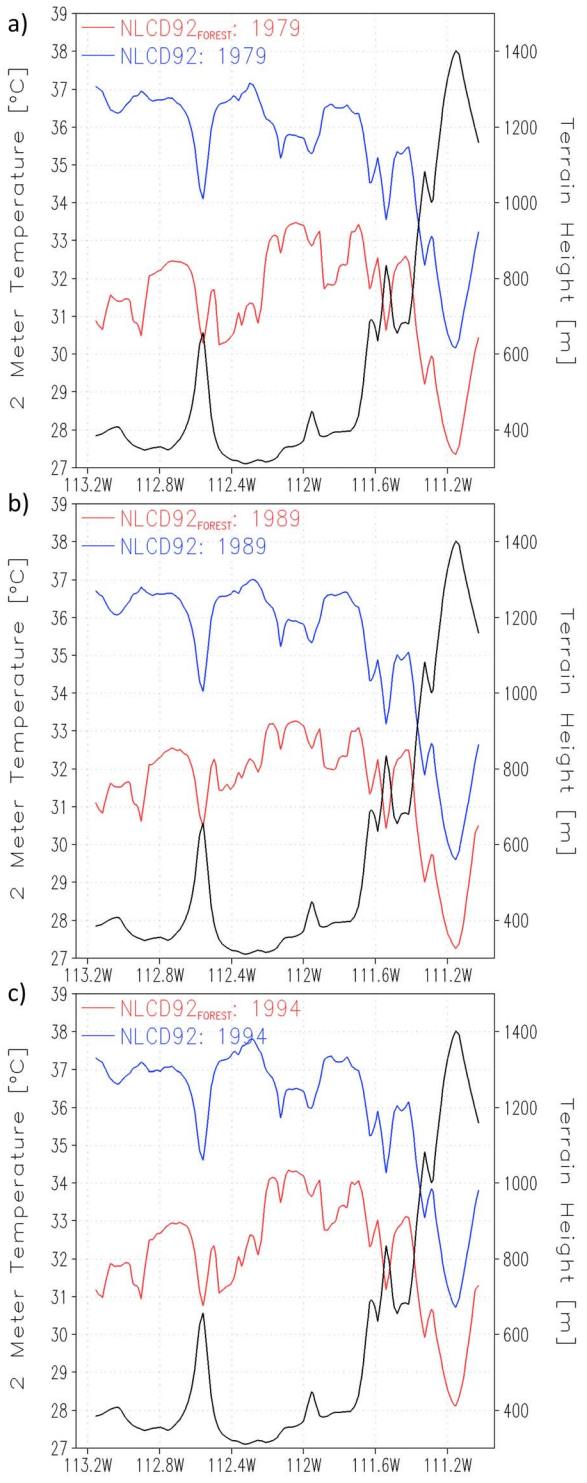

Figure 9. As Figure 8 but for NLCD92 scenarios (solid blue line) and $NLCD92_{FOREST}$ scenarios (solid red line) for (a) 1979, (b) 1989, and (c) 1994.

of 112.6°W is related to changes in topography; this is also the case east of about 111.7°W. Differences in near-surface temperatures among the paired simulations (for all three simulated Julys) begin as one proceeds toward the irrigated agriculture region, with warming for the sparsely vegetated desert (i.e., presettlement scenario) relative to irrigated agriculture (i.e., the NLCD92 scenario) of a couple of tenths of a degree Celsius. Continued progression eastward (e.g., to about 112.2°W, where one is firmly entrenched within the urban area) results in a further and relatively larger decrease in temperature (compared with the progression from semidesert land to irrigated agriculture land). While surface-absorbed energy was efficiently used to heat the near-surface air over the vegetation-sparse and water-limited semidesert simulated in the presettlement scenarios, there is significantly less energy used to heat air over the urban region, in large part because of the enhanced heat storage of the built environment (see section 3.3). The region where urbanization occurred also coincided with the lowest cross-sectional elevation, resulting in the largest near-surface temperature contrasts between the presettlement and NLCD92 simulations. These differences are consistent among the differently simulated Julys, and the molar-shaped temperature pattern for each of the modern-day landscapes (i.e., NLCD92 for each of the trio of Julys) is lower relative to the surrounding semidesert (e.g., west of 112.4°W and east of about 111.9°W, notwithstanding temperature variability that is due to topography).

[33] We posit that the decrease in daytime temperature over the urban area (relative to outlying areas) noted upon urbanization (i.e., the simulated cooling) occurs because of greater heating rates in the surrounding semidesert and is related to the biome in which the city resides and not to any unique features of metro Phoenix. To test this hypothesis, we conducted three additional simulations using the modern-day representation of greater Phoenix with the following changes. We altered the surrounding semidesert biome to a temperate broadleaf forest biome that is more distinctive of major urban areas in, for example, the northeastern United States. To do this, the shrubland category surrounding metro Phoenix was replaced with an evergreen broadleaf landscape. The sparse vegetation (generally at 20% vegetation fraction or less) of the semidesert is not fitting for a temperate broadleaf forest biome and consequently required modification. The vegetation fraction was set to a constant value of 90% for the broadleaf forest and irrigated agriculture categories (this agrees well with July forest coverage west of, for example, Boston, Massachusetts, and with July vegetation coverage of agricultural areas in the Midwest United States) [*Gutman and Ignatov*, 1998]. Last, the initial soil moisture value was increased by 75% for all soil layers to more accurately represent the nondesiccated soils of a temperate broadleaf landscape. All other settings remained identical to the trio of NLCD92 simulations, including irrigation frequency within the urban area and over irrigated agriculture locations.

[34] Figure 9, presented in a fashion similar to that of Figure 8, shows results of the new NLCD92 experiments with metro Phoenix located within a temperate broadleaf forest biome (hereafter referred to as $NLCD92_{FOREST}$) alongside the previously documented NLCD92 simulations, with metro Phoenix located within its natural semidesert environment. The general trend of lower near-surface air temperatures is apparent for $NLCD92_{FOREST}$ compared with NLCD92. This result is not surprising given the repartitioning toward greater latent relative to sensible heating.

Notably, the urban area is no longer cooler than its surrounding environment. Rather, for each of the trio of simulated Julys, metro Phoenix is as warm or warmer than its neighboring surroundings, as the rapid daytime heating over the parched semidesert adjoining Phoenix has been replaced with a landscape that warms gradually, in a manner more appropriate for temperate regions.

4. Discussion and Concluding Remarks

[35] We have performed an evaluation of and sensitivity to anthropogenic LULCC using the WRF regional climate model, applied over the semiarid and water-vulnerable Phoenix metropolitan area, with emphasis on the depiction of the evolving diurnal cycle of near-surface temperatures and representation of the urban area's daytime cool island.

[36] Our results demonstrate an excellent depiction of the daily and monthly evolution of the midsummer diurnal cycle with WRF. Low-level thermal day-to-day variability, monthly averaged composite diurnal cycles, and standard deviations (relative to observations) illustrate the correct representation of the semiarid region's harsh summer climate. The proper simulation of peak daytime temperature timing is of particular importance to hot and arid urban areas such as Phoenix that require accurate and timely profiles of peak energy demand associated with basic human adaptation and function.

[37] Although near-surface temperature sensitivity to anthropogenic LULCC is small on the regional scale, our experiments, supported by previous observational analyses, show two distinct and opposing impacts on the urbanized diurnal cycle during the extent of the full day, with evening and nighttime warming (relative to the undeveloped semidesert landscape) partially offset by daytime cooling. To our knowledge, these are the first simulations to explicitly depict the daytime cooling effect of the urbanizing metro Phoenix landscape.

[38] Analysis of the surface energy budget components indicates a shift toward greater latent heating for regions undergoing a change to irrigated agriculture and enhanced heat storage for regions undergoing urbanization. The slow release of stored daytime heat and enhanced emission of longwave radiation toward the surface (from within the urban canopy) for urbanizing areas during the evening and nighttime hours is largely responsible for the nighttime warming influence. This result is in agreement with previous modeling [e.g., *Grossman-Clarke et al.*, 2005] and observationally based research [e.g., *Brazel et al.*, 2000]. Contrary to prior speculation, however, our results do not indicate a significant impact on near-surface temperatures (and surface energy budget components) because of irrigation within urban areas, suggesting that the oasis effect is not the principal mechanism explaining the urban area's daytime cooling.

[39] To determine the cause of the observed and simulated cooling, the semidesert biome within which greater Phoenix resides was replaced with a temperate broadleaf forest biome. Modification of metro Phoenix's surrounding environment eliminated the urban cooling entirely, suggesting that adjacent conditions (e.g., soil moisture, land cover) play a principal role in establishing the nature and evolution of the diurnal cycle of near-surface temperatures for the metro area. This result is in agreement with recent observationally based evidence showing the dependence of the UHI of diverse cities across the United States on differing ecological settings and environmental factors [*Imhoff et al.*, 2010]. The precise impact of urbanization on the diurnal cycle of near-surface temperatures largely depends on the surrounding environment in which urbanization occurs, including landscape and soil moisture conditions, rather than any distinguishing features of the city itself.

[40] Future work quantifying the impact of urbanization on the diurnal cycle of near-surface temperatures should focus on other rapidly expanding, and water-vulnerable, semiarid metropolitan regions (e.g., Las Vegas, Nevada, or Riyadh, Saudi Arabia). It is plausible that urbanization impacts on the diurnal cycle illustrate similar daytime cooling and nighttime warming (of greater relative magnitude) as documented over metro Phoenix, potentially distinguishing general urbanization effects over semiarid metropolitan regions from their counterparts in temperate zones.

[41] Given further anticipated urban expansion and LULCC over many regions, attention should also be given to sustainably built urban forms [*Jo et al.*, 2010; *Seto et al.*, 2010] that mitigate the severity of urban-induced warming. This is important for many currently developing metropolitan regions, but is especially critical for water-vulnerable metro areas such as Phoenix. These urban hubs are currently facing significant water sustainability concerns that are due to the rising demands associated with rapid population increase [*Gober and Kirkwood*, 2010], with stringent urban adaptation measures potentially resulting in future allocation reductions.

[42] **Acknowledgments.** This work was funded by NSF grant ATM-0934592.

References

Anyah, R. O., C. P. Weaver, G. Miguez-Macho, Y. Fan, and A. Robock (2008), Incorporating water table dynamics in climate modeling: 3. Simulated groundwater influence on coupled land-atmosphere variability, *J. Geophys. Res.*, *113*, D07103, doi:10.1029/2007JD009087.

Arnfield, A. J. (2003), Two decades of urban climate research: A review of turbulence, exchanges of energy and water, and the urban heat island, *Int. J. Climatol.*, *23*, 1–26, doi:10.1002/joc.859.

Balling, R. C., Jr., and S. W. Brazel (1987), Time and space characteristics of the Phoenix urban heat island, *J. Ariz. Nev. Acad. Sci.*, *21*, 75–81.

Balling, R. C., Jr., R. S. Cerveny, and C. D. Idso (2001), Does the urban CO_2 dome of Phoenix, Arizona contribute to its heat island?, *Geophys. Res. Lett.*, *28*, 4599–4601, doi:10.1029/2000GL012632.

Barnett, T. P., and D. W. Pierce (2008), When will Lake Mead go dry?, *Water Resour. Res.*, *44*, W03201, doi:10.1029/2007WR006704.

Bornstein, R. D. (1968), Observations of the urban heat island effect in New York City, *J. Appl. Meteorol.*, *7*, 575–582, doi:10.1175/1520-0450(1968)007<0575:OOTUHI>2.0.CO;2.

Brazel, A., N. Selover, R. Vose, and G. Heisler (2000), The tale of two climates–Baltimore and Phoenix urban LTER sites, *Clim. Res.*, *15*, 123–135, doi:10.3354/cr015123.

Chen, F., and J. Dudhia (2001), Coupling an advanced land-surface/hydrology model with the Penn State/NCAR MM5 modeling system. Part I: Model description and implementation, *Mon. Weather Rev.*, *129*, 569–585, doi:10.1175/1520-0493(2001)129<0569:CAALSH>2.0.CO;2.

Cheval, S., and A. Dumitrescu (2009), The July urban heat island of Bucharest as derived from MODIS images, *Theor. Appl. Climatol.*, *96*, 145–153, doi:10.1007/s00704-008-0019-3.

Csiszar, I., and G. Gutman (1999), Mapping global land surface albedo from NOAA AVHRR, *J. Geophys. Res.*, *104*, 6215–6228, doi:10.1029/1998JD200090.

Erie, L. J., O. F. French, D. A. Bucks, and K. Harris (1982), Consumptive use of water by major crops in the Southwestern United States, *Agric.*

Res. Ser. Conserv. Res. Rep. 29, 40 pp., U.S. Dep. of Agric., Washington, D. C.

Fast, J. D., J. C. Torcolini, and R. Redman (2005), Pseudovertical temperature profiles and the urban heat island measured by a temperature datalogger network in Phoenix, Arizona, *J. Appl. Meteorol.*, *44*, 3–13, doi:10.1175/JAM-2176.1.

Gammage, G., Jr., J. S. Hall, R. E. Lang, R. Melnick, and N. Welch (2008), *Megapolitan: Arizona's Sun Corridor*, Morrison Institute for Public Policy, Ariz. State Univ., Tempe.

Gedzelman, S. D., S. Austin, R. Cermak, N. Stefano, S. Partridge, S. Quesenberry, and D. A. Robinson (2003), Mesoscale aspects of the urban heat island around New York City, *Theor. Appl. Climatol.*, *75*, 29–42.

Georgescu, M. (2008), Evaluating the effect of land-use and land-cover change on climate in the greater Phoenix, AZ, region, Ph.D. dissertation, Ariz. State Univ., Tempe.

Georgescu, M., G. Miguez-Macho, L. T. Steyaert, and C. P. Weaver (2008), Sensitivity of summer climate to anthropogenic land-cover change over the Greater Phoenix, AZ, region, *J. Arid Environ.*, *72*, 1358–1373, doi:10.1016/j.jaridenv.2008.01.004.

Georgescu, M., G. Miguez-Macho, L. T. Steyaert, and C. P. Weaver (2009), Climatic effects of 30 years of landscape change over the Greater Phoenix, AZ, region: 1. Surface energy budget changes, *J. Geophys. Res.*, *114*, D05110, doi:10.1029/2008JD010745.

Gober, P. A., and C. W. Kirkwood (2010), Vulnerability assessment of climate-induced water shortage in Phoenix, *Proc. Natl. Acad. Sci. U. S. A.*, *107*, 21,295–21,299, doi:10.1073/pnas.0911113107.

Golden, J., A. Brazel, J. Salmond, and D. Laws (2006), Energy and water sustainability: The role of urban climate change from metropolitan infrastructure, *J. Eng. Sustain. Dev.*, *1*, 55–70.

Golden, J. S., D. Hartz, A. Brazel, G. Luber, and P. Phelan (2008), A biometeorology study of climate and heat-related morbidity in Phoenix from 2001 to 2006, *Int. J. Biometeorol.*, *52*, 471–480, doi:10.1007/s00484-007-0142-3.

Grimm, N. B., and C. L. Redman (2004), Approaches to the study of urban ecosystems: The case of central Arizona-Phoenix, *Urban Ecosyst.*, *7*, 199–213, doi:10.1023/B:UECO.0000044036.59953.a1.

Grimm, N. B., D. Foster, P. Groffman, J. M. Grove, C. S. Hopkinson, K. J. Nadelhoffer, D. E. Pataki, and D. P. C. Peters (2008), The changing landscape: Ecosystem responses to urbanization and pollution across climatic and societal gradients, *Front. Ecol. Environ*, *6*(5), 264–272, doi:10.1890/070147.

Grimmond, C. S. B., and T. R. Oke (1999), Heat storage in urban areas: Local-scale observations and evaluation of a simple model, *J. Appl. Meteorol.*, *38*, 922–940, doi:10.1175/1520-0450(1999)038<0922:HSIUAL>2.0.CO;2.

Grossman-Clarke, S., J. A. Zehnder, W. L. Stefanov, Y. Liu, and M. A. Zoldak (2005), Urban modifications in a mesoscale meteorological model and the effects on near-surface variables in an arid metropolitan region, *J. Appl. Meteorol.*, *44*, 1281–1297, doi:10.1175/JAM2286.1.

Gutman, G., and A. Ignatov (1998), The derivation of green vegetation fraction from NOAA/AVHRR data for use in numerical weather prediction models, *Int. J. Remote Sens.*, *19*, 1533–1543, doi:10.1080/014311698215333.

Hamming, R. W. (1983), *Digital Filters*, Prentice-Hall, Englewood Cliffs, N. J.

Hansen, J., R. Ruedy, J. Glascoe, and M. Sato (1999), GISS analysis of surface temperature change, *J. Geophys. Res.*, *104*(D24), 30,997–31,022, doi:10.1029/1999JD900835.

Harlan, S. L., A. Brazel, G. D. Jenerette, N. S. Jones, L. Larsen, L. Prashad, and W. L. Stefanov (2008), In the shade of affluence: The inequitable distribution of the urban heat island, *Res. Soc. Probl. Public Policy*, *15*, 173–202, doi:10.1016/S0196-1152(07)15005-5.

Hawkins, T. W., A. J. Brazel, W. L. Stefanov, W. Bigler, and E. M. Saffell (2004), The role of rural variability in urban heat island determination for Phoenix, Arizona, *J. Appl. Meteorol.*, *43*, 476–486, doi:10.1175/1520-0450(2004)043<0476:TRORVI>2.0.CO;2.

Higgins, R. W., et al. (2000), Improved US precipitation quality control system and analysis, *NCEP/Clim. Predict. Cent. ATLAS 7*, 40 pp., Natl. Cent. for Environ. Predict., Camp Springs, Md.

Hsu, S. I. (1984), Variation of an urban heat island in Phoenix, *Prof. Geogr.*, *36*, 196–200, doi:10.1111/j.0033-0124.1984.00196.x.

Imhoff, M. L., P. Zhang, R. E. Wolfe, and L. Bounoua (2010), Remote sensing of the urban heat island effect across biomes in the continental USA, *Remote Sens. Environ.*, *114*, 504–513, doi:10.1016/j.rse.2009.10.008.

Jacobson, M. Z. (2010), Enhancement of local air pollution by urban air domes, *Environ. Sci. Technol.*, *44*, 2497–2502, doi:10.1021/es903018m.

Jo, J. H., J. Carlson, J. S. Golden, and H. Bryan (2010), Sustainable urban energy: Development of a mesoscale assessment model for solar reflective roof technologies, *Energ. Policy*, *38*, 7951–7959, doi:10.1016/j.enpol.2010.09.016.

Kain, J. S. (2004), The Kain–Fritsch convective parameterization: An update, *J. Appl. Meteorol.*, *43*, 170–181, doi:10.1175/1520-0450(2004)043<0170:TKCPAU>2.0.CO;2.

Knowles-Yanez, K., C. Moritz, J. Fry, C. L. Redman, M. Bucchin, and P. H. McCartney (1999), Historic Land Use Team: Phase I Report on Generalized Land Use, *Cent. Ariz.–Phoenix Long-Term Ecol. Res. Contrib. 1*, 21 pp., Arizona State Univ., Tempe.

Kusaka, H., and F. Kimura (2004), Thermal effects of urban canyon structure on the nocturnal heat island: Numerical experiment using a mesoscale model coupled with an urban canopy model, *J. Appl. Meteorol.*, *43*, 1899–1910, doi:10.1175/JAM2169.1.

Landsberg, H. E. (1981), *The Urban Climate*, 278 pp., Academic, San Diego, Calif.

Lo, J. C. F., A. K. H. Lau, F. Chen, J. C. H. Fung, and K. K. M. Leung (2007), Urban modification in a mesoscale model and the effects on the local circulation in the Pearl River Delta region, *J. Appl. Meteorol. Climatol.*, *46*, 457–476, doi:10.1175/JAM2477.1.

Loridan, T., C. S. B. Grimmond, S. Grossman-Clarke, F. Chen, M. Tewari, K. Manning, A. Martilli, H. Kusaka, and M. Best (2010), Trade-offs and responsiveness of the single-layer urban canopy parametrization in WRF: An offline evaluation using the MOSCEM optimization algorithm and field observations, *Q. J. R. Meteorol. Soc.*, *136*, 997–1019, doi:10.1002/qj.614.

Mesinger, F., et al. (2006), North American regional reanalysis, *Bull. Am. Meteorol. Soc.*, *87*, 343–360, doi:10.1175/BAMS-87-3-343.

Oke, T. R. (1973), City size and the urban heat island, *Atmos. Environ.*, *7*, 769–779, doi:10.1016/0004-6981(73)90140-6.

Oke, T. R. (1981), Canyon geometry and the nocturnal urban heat island: Comparison of scale model and field observations, *J. Climatol.*, *1*, 237–254, doi:10.1002/joc.3370010304.

Oke, T. R. (1987), *Boundary Layer Climates*, 2nd ed., 435 pp., Methuen, London.

Oke, T. R., and G. B. Maxwell (1975), Urban heat island dynamics in Montreal and Vancouver, *Atmos. Environ.*, *9*, 191–200, doi:10.1016/0004-6981(75)90067-0.

Pielke, R. A. (2001), Influence of the spatial distribution of vegetation and soils on the prediction of cumulus convective rainfall, *Rev. Geophys.*, *39*, 151–177, doi:10.1029/1999RG000072.

Potchter, O., P. Cohen, and A. Bitan (2006), Climatic behavior of various urban parks during hot and humid summer in the Mediterranean city of Tel Aviv, Israel, *Int. J. Climatol.*, *26*, 1695–1711, doi:10.1002/joc.1330.

Rajagopalan, B., K. Nowak, J. Prairie, M. Hoerling, B. Harding, J. Barsugli, A. Ray, and B. Udall (2009), Water supply risk on the Colorado River: Can management mitigate?, *Water Resour. Res.*, *45*, W08201, doi:10.1029/2008WR007652.

Sailor, D. J. (1995), Simulated urban climate response to modification in surface albedo and vegetative cover, *J. Appl. Meteorol.*, *34*, 1694–1704, doi:10.1175/1520-0450-34.7.1694.

Seto, K. C., R. Sanchez-Rodriguez, and M. Fragkias (2010), The new geography of contemporary urbanization and the environment, *Annu. Rev. Environ. Resour.*, *35*, 167–194, doi:10.1146/annurev-environ-100809-125336.

Skamarock, W. C., and J. B. Klemp (2008), A time-split nonhydrostatic atmospheric model for research and NWP applications, *J. Comput. Phys.*, *227*, 3465–3485, doi:10.1016/j.jcp.2007.01.037.

Skamarock, W. C., J. B. Klemp, J. Dudhia, D. O. Gill, D. M. Barker, M. G. Duda, X.-Y. Huang, W. Wang, and J. G. Powers (2008), A description of the advanced research WRF version 3, *NCAR Tech. Note NCAR/TN–475+STR*, 125 pp., Natl. Cent. for Atmos. Res., Boulder, Colo.

Spronken-Smith, R. A., T. R. Oke, and W. P. Lowry (2000), Advection and the surface energy balance across an irrigated urban park, *Int. J. Climatol.*, *20*, 1033–1047, doi:10.1002/1097-0088(200007)20:9<1033::AID-JOC508>3.0.CO;2-U.

Stabler, L. B., C. A. Martin, and A. J. Brazel (2005), Microclimates in a desert city were related to land use and vegetation index, *Urban For. Urban Green.*, *3*, 137–147, doi:10.1016/j.ufug.2004.11.001.

Taha, H. (1997), Urban climates and heat islands: Albedo, evapotranspiration, and anthropogenic heat, *Energy Build.*, *25*, 99–103, doi:10.1016/S0378-7788(96)00999-1.

Taha, H., H. Akbari, and A. Rosenfeld (1991), Heat island and oasis effects of vegetative canopies: Micrometeorological field measurements, *Theor. Appl. Climatol.*, *44*, 123–138, doi:10.1007/BF00867999.

Tarleton, L. F., and R. W. Katz (1995), Statistical explanation for trends in extreme summer temperatures at Phoenix, Arizona, *J. Clim.*, *8*, 1704–1708, doi:10.1175/1520-0442(1995)008<1704:SEFTIE>2.0.CO;2.

Tran, H., D. Uchihama, S. Ochi, and Y. Yasuoka (2006), Assessment with satellite data of the urban heat island effects in Asian mega cities, *Int. J. Appl. Earth Obs. Geoinf.*, *8*, 34–48, doi:10.1016/j.jag.2005.05.003.

Vogelmann, J. E., S. M. Howard, L. Yang, C. R. Larson, B. K. Wylie, and J. N. Van Driel (2001), Completion of the 1990s National Land Cover Data Set for the conterminous United States, *Photogramm. Eng. Remote Sens.*, *67*, 650–662.

Zehnder, J. A. (2002), Simple modifications to improve fifth-generation Pennsylvania State University-National Center for Atmospheric Research Mesoscale Model performance for the Phoenix, Arizona, metropolitan area, *J. Appl. Meteorol.*, *41*, 971–979, doi:10.1175/1520-0450(2002)041<0971:SMTIFG>2.0.CO;2.

Zhou, L., R. E. Dickinson, Y. Tian, J. Fang, Q. Li, R. K. Kaufmann, C. J. Tucker, and R. B. Myneni (2004), Evidence for a significant urbanization effect on climate in China, *Proc. Natl. Acad. Sci. U. S. A.*, *101*(26), 9540–9544, doi:10.1073/pnas.0400357101.

J. Dudhia, Mesoscale and Microscale Meteorology Division, National Center for Atmospheric Research, PO Box 3000, Boulder, CO 80307–3000, USA.

M. Georgescu, A. Mahalov, and M. Moustaoui, School of Mathematical and Statistical Sciences, Center for Environmental Fluid Dynamics, Global Institute of Sustainability, Arizona State University, Tempe, AZ 85287, USA. (matei.georgescu@asu.edu)